Supplementary Data 1: CO_2 emission data

CO_2 concentration measurement

We measured the emission of CO_2 released from deforming specimens using a solid electrolyte-type CO_2 sensor (TGS4161 with an accuracy of about 20 %; Figaro Co. Ltd., Osaka, Japan). Commercially available sensors of this type have a zeolite filter that excludes the influence of other gases present in the atmosphere. However, this filter delays the response of the sensor. Thus, for the experiments in this study, we used a sensor without such a filter. In this case, it took the sensor about 0.9-1.0 seconds to yield an initial DC output. The sensor output in DC was then converted with an IC circuit into CO_2 concentration in ppm. It takes about 90 seconds to give outputs corresponding to the 90% of CO_2 concentration when the sensor is instantly exposed to an atmosphere with a different CO_2 concentration.

The CO_2 sensor was positioned about 10 cm away from the specimen, on a corner of the specimen chamber sealed with in-permeation tapes. There is a delay between the time of CO_2 emission initiation within the deforming sample and the recorded CO_2 data due to sensor response, CO_2 travel distance, gouge permeability and sample assembly configuration (sealing of Teflon ring). Since this time delay is difficult to be estimated, it is only possible to have an overestimated time initiation for CO_2 emissions from the sample (i.e., it is likely that CO_2 production within the slip zone of the sample initiated earlier than what the CO_2 sensor in the chamber could detect).

During our experiments, we could not directly measure the CO_2 concentration in the slip zone, but could only monitor the CO_2 gas escaping from the slip zone through the gouge layer and the space between the Teflon and the host rocks.

Supplementary Data 2: Microstructural observations of decomposed material

In an atmosphere of CO_2, dolomite $MgCa(CO_3)_2$ starts to decompose to $Ca_xMg_{1-x}CO_{3(Mg.rich\ calcite)}$ + $MgO_{(periclase)}$+ $CO_{2(fluid)}$ at temperatures of about 550°C and Mg-rich calcite ($Ca_xMg_{1-x})CO3$ decomposes to CaO $_{(lime)}$ + MgO $_{(periclase)}$ + $CO_{2(fluid)}$ at temperatures of about 700 to 900°C (Samtani et al., *Journal of Thermal Analysis and Calorimetry* **65**, 93-101, 2001). There is a general agreement in the literature about the fact that, during heating experiments on dolomite, $CaCO_3$ starts to be detected at temperatures of about 550°C (Hashimoto et al., *Journal of Solid State Chemistry,* **33**, 181-188, 1980), while MgO is not yet detectable (De Aza et al., *Journal of American Ceramic Society,* **85**, 881-888, 2002). In particular, calcite/Mg-rich calcite crystals are relatively large soon after their formation and remain constant in size during the isothermal decomposition of dolomite. On the contrary, periclase nucleates in an amorphous to poorly crystalline state and it grows very slowly, resulting into much smaller grain size than calcite (Hashimoto et al., *Journal of Solid State Chemistry,* **33**, 181-188, 1980).

XRPD analyses of the entire gouge layer deformed during our experiments revealed the presence of partial thermal decomposition products of dolomite as Mg-rich calcite and periclase (Supplementary Figure 3). Minor fluorite (CaF_2), detected by XRPD patterns, has been interpreted as the result of the reaction between dolomite and fluorine, the latter produced by thermal decomposition of small pieces of Teflon (C_2F_4) accidentally included in the gouge layer during the experiments and/or sample preparation.

TEM observations in the slip zone show a close association of rounded ultra-fine crystals, with relatively constant grain size, from few nano meters up to 20 nm in diameter (low-magnification images, Supplementary Figure 4). Grain boundaries are often ill-defined, but they locally evolve to mature, polygonalized patterns. The resulting nanotexture is compact and porosity-free (Supplementary Figure 4).

Measured d_{hkl} spacings from most intense diffraction rings are

dol										cal	hkl
2.886	2.86	2.88	2.91	2.94	2.94	2.96	3.00	3.03			104
2.405	2.41	2.38	2.41	2.41	2.42	2.42	2.49	2.49			110
2.192	2.19	2.19	2.21	2.22	2.22	2.23	2.28	2.28			113
2.015				2.02	2.01	2.02	2.04			2.09	202
1.786	1.81	1.79			1.82				1.85	1.87	116

where the d-spacings for reference dolomite (dol, MPDF 11-78) and calcite (cal, MPDF 24-27) are also reported for comparison, together with corresponding hkl indexes. All measured rings can be attributed to $Ca_{0.5}Mg_{0.5}CO_3$ - $CaCO_3$ phases. The observed range in d-spacing values (i.e., from 2.86 to 3.00 Å for d_{104}) reflects variable Mg/Ca ratios; some diffraction patterns indicate predominant dolomite, whereas others have larger d-spacings, indicating predominant calcite (or Mg-rich calcite), in agreement with XRPD analyses.

High-magnification TEM images in Supplementary Figure 4 show that that interstitial material is usually absent and that lattice fringes from nearby crystals are often overlapped, producing typical Moiré patterns. Lattice fringes have variable orientation/spacing, confirming randomly oriented textures (Supplementary Figure 4), and form defect-free, regular sequences (Supplementary Figure 4). Overall evidences (e.g., the ultra-fine grain size, the variable crystal orientation, the occurrence of polygonalized boundaries and the absence of defective structures) suggest a significant structural reorganization of the material in the slip zone.

The collection of pure, uncontaminated EDS data (Energy Dispersive Spectrometry) was hampered by the ultra-fine grain size of the slip material. TEM observations were able to detect phases that can be interpreted as calcite or Mg-rich calcite but it was not possible to have good quality data about the observation of the periclase, although its presence has been detected by XRPD analyses. We interpret this as possibly due to the fact that periclase, as reported in the literature (Hashimoto et al., *Journal of Solid State Chemistry,* **33**, 181-188, 1980, De Aza et al., *Journal of American Ceramic Society,* **85**, 881-888, 2002), may have formed during the initial stages of the thermal decomposition of dolomite (T = 550°C) as an ultra-fine low crystallinity phase, that, due to the short duration of the experiments, had not sufficient time to develop into a crystalline phase with a grain size large enough to be detected by TEM observations.

Supplementary Data 3: CO_2 emission data, temperature rise and slip weakening mechanisms

During experiments on dry and water saturated dolomite, CO_2 emissions have been recorded after few seconds from the beginning of slip (Figs. 1A-C in the main text). For v = 1.3 m/s and $\sigma_n \leq 0.8$ MPa, only very minor amount of CO_2 emissions were recorded after 4.9s from the beginning of the experiment (Fig. 1A in the main text). For v = 1.3 m/s and $\sigma_n > 0.8$ MPa, CO_2 emissions start after 4.17s from the beginning of the experiment and increase according to an initial linear trend followed by an exponential one (Fig. 1B in the main text).

Although there is a time lag between the initiation and the actual measurement of the CO_2 emissions, in both experiments the initiation of CO_2 emissions was recorded during the transient stage of the shear stress decay to steady state values (Figs. 1A-C in the main text). If we consider that dolomite $MgCa(CO_3)_2$ starts to decompose to $Ca_xMg_{1-x}CO_{3(Mg.rich\ calcute)}$ + $MgO_{(periclase)}$+ $CO_{2(fluid)}$ at temperatures of about 550°C and Mg-rich calcite $(Ca_xMg_{1-x})CO_3$ decomposes to $CaO_{(lime)}$ + $MgO_{(periclase)}$ + $CO_{2(fluid)}$ at temperatures of about 700 to 900°C (Samtani et al., *Journal of Thermal Analysis and Calorimetry* **65**, 93-101, 2001), our CO_2 data suggest that temperatures in excess of T = 550ºC were reached within the slip zone before steady state weakening was attained.

During the experiments performed at constant slip rate v, the frictional strength decays with slip x according to an exponential law (Mizoguchi et al., *Geophys. Res. Lett.* **34,** doi:10.1029/2006GL027931, 2007). A rough estimation of the average temperature T_{Av} attained within a slip zone with zero thickness, at the end of the transient stage when $d = D_w$, is given by (Carslaw and Jaeger, Conduction of Heat in Solids, 2nd edition, 1959)

$$T_{Av}\left(d = D_w\right) = \frac{\tau_{av}\sqrt{D_w v}}{\rho\ c_p\sqrt{\pi\kappa}} \qquad \text{Eq. 1}$$

where d is the displacement, D_w is the slip weakening distance, τ_{av} is the average shear strength during the transient stage ($\tau_{ss} < \tau_f < \tau_p$), ρ is the rock density, c_p is the specific heat capacity and κ is the thermal diffusivity.

Upon solving Eq. 1 for our experimental conditions (see Supplementary Table 1) and by using for a temperature of 473 K, c_p = 1072 Jkg^{-1} K^{-1}and κ = 1.15*10^{-6} m^{2}s^{-1} and for a temperature of 773 K, c_p = 1249 J kg^{-1} K^{-1} and κ = 1.0*10^{-6} m^{2}s^{-1} (thermal data from Holland and Powell, *J. Met. Geol.,* **8**, 89-124, 1990 and Clauser and Hunges, *Rocks Physics and Phase Relations.* **AGU Vol. 3**, 105-126, 1995), we obtain that the estimated average temperature increase in the slip zone, at the end of the transient stage and considering the ambient temperature of 25ºC for two experiments, is $T_{Av\ \mathrm{HVR1160}}$ = 275ºC and $T_{Av\ \mathrm{HVR1165}}$ = 379ºC, respectively.

Eq. 1 estimates the average temperature and it does not consider the slip rate gradient in the slipping zone from the inner (v = 0) to the external part of the sample (Supplementary Fig. 2, Eq. 1). For instance, if we solve Eq. 1 in the case of experiment HVR1164 for a slip rate of 2 m/s achieved at the edge of the gouge layer (v = 25 rps * 12.5 mm of sample radius), then the estimated temperature at the end of the transient stage is $T_{Max\ \mathrm{HVR1165}}$ = 460^{o}C. This maximum temperature obtained at the edge of the sample is very close but lower than the critical temperature T = 550 ^{o}C necessary to initiate the thermal decomposition processes of dolomite (Samtani et al., *Journal of Thermal Analysis and Calorimetry* **65**, 93-101, 2001). Temperature calculation at the edge of the sample is qualitatively in accord with microstructural observations from all the samples tested in this study, which show the localization of decarbonation processes at the outer edges of the samples, where the highest values of slip rates are achieved.

Slip weakening occurs from the beginning of the transient stage and so at slip zone bulk temperatures below the temperature necessary to activate the thermal decomposition of the dolomite (T_{dol} = 550ºC). One possible explanation is that the temperature within the slip zone was only locally risen above the dolomite thermal decomposition temperature (T = 550ºC) by flash heating processes at microcontact asperities, active during the early transient stage (Rice, J. , *J. Geophys. Res.* **111,** doi:10.1029/2005JB004006, 2006). The critical weakening velocity v_w *is the velocity* necessary to produce the flash temperature rise required to decompose the dolomite gouge *,* for a given contact dimension of grains (ϕ). It can be estimated, as a very rough and simplified first approximation (i.e., it implies that fault surface roughness and asperity population are not altered by wear, formation of gouge and rolling of grains during slip), by (Rice, J., *J. Geophys. Res.* **111,** doi:10.1029/2005JB004006, 2006; Beeler et al., *J. Geophys. Res.* **113,** doi:10.1029/2007JB004988, 2008)

$$v_w = \frac{\pi\alpha}{\phi}\left[\frac{\rho C_p\left(T_{dol} - T_{init}\right)}{\tau_{asp}}\right]^2 \qquad \text{Eq. 2}$$

where T_{dol} is the temperature at which the dolomite starts to decompose, T_{init} is the initial temperature and τ_{asp} is the frictional contact shear strength. For T_{dol} = 550 ºC, T_{init} = 20 ºC and $\tau_c = \mu * \sigma_y = 1.31*10^9$, Eq. 2 returns the critical velocities v_w for any contact dimension ϕ of the grains in the slip zone (μ = 0.6, from Weeks and Tullis, *J. Geophys. Res.* **90,** 7821-7826, 1985, and $\sigma_y = 2.19*10^9$, from Broz et al., *Am. Mineral.,* **91**, 135-142, 2006, are the frictional coefficient and the microindentation hardness of dolomite, respectively). The critical weakening velocities v_w calculated by Eq. 2 have been plotted vs. average grain size ϕ of the slip zone in the diagram in Figure 3C of the main text. The integration of calculated v_w data with microstructural observations from experiments performed at different displacements d (Fig. 2 in the main text), suggest that flash heating was not the main dynamic slip weakening process in operation at our experimental conditions as it would have been inhibited very soon for displacements $d < D_w$, when intense grain size reduction by both cataclastic and chemical/thermal processes took place.

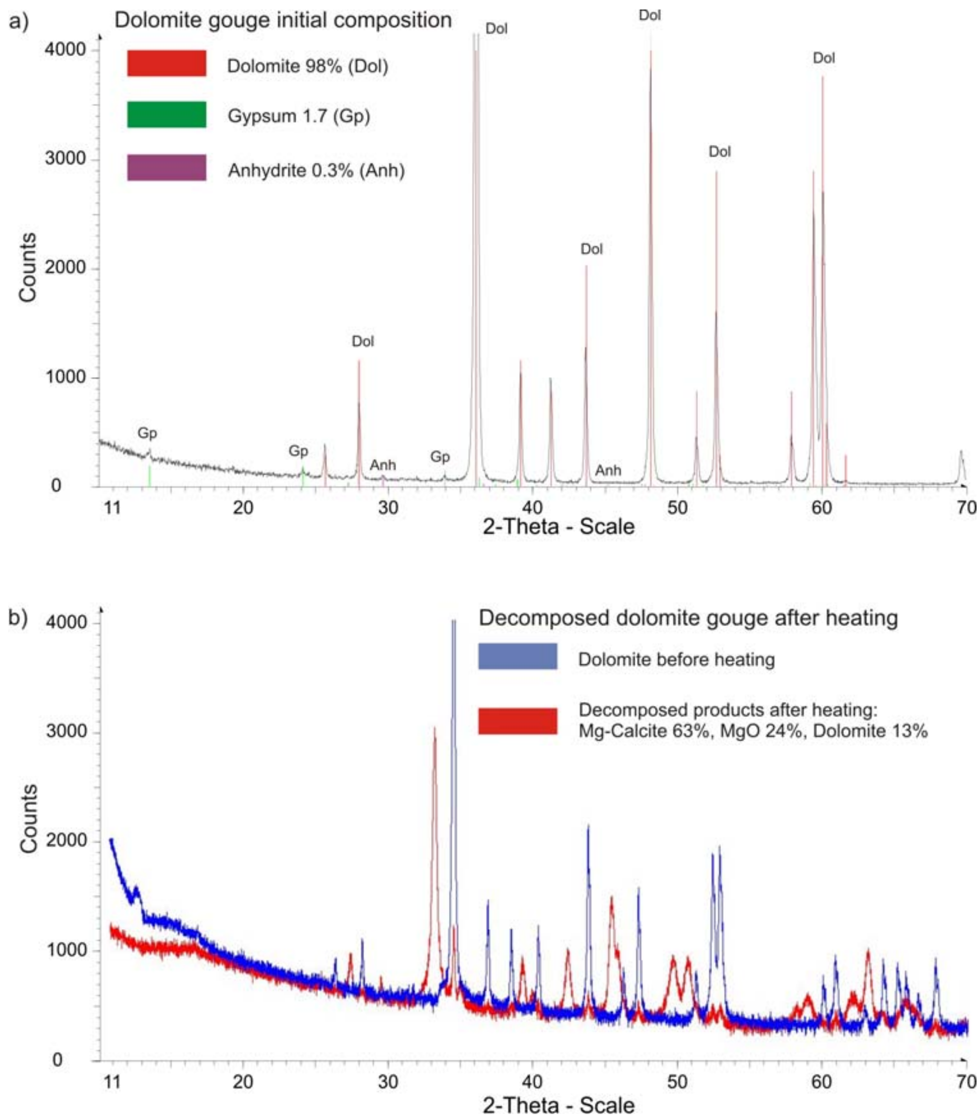

Supplementary Figure DR1: Composition of initial gouge material. a. The composition of the initial dolomite-rich gouge, used during our dry and distilled water saturated experiments is 98% dolomite $MgCa(CO_3)_2$, 1.7% Gypsum ($CaSO_4$*$2H_2O$) and 0.3% Anhydrite ($CaSO_4$), as shown by the results of X-ray powder diffraction (XRPD) semi-quantitative analyses (%weight). This fault gouge material has been used for the experiments to simulate seismic slip in natural faults. **b.** Initially pure dolomite has been heated in a vented oven from 20°C to 650°C in 20 minutes, kept at 650°C for 5 hours and finally cooled to 20°C in 90 minutes. After heating treatment, the dolomite gouge material decomposed to 63% Mg-rich calcite $(Ca_{0.936}Mg_{0.064})CO_3$, 24% periclase ($MgO$) and some residual 13% dolomite $MgCa(CO_3)_2$, as shown by the results of XRPD semi-quantitative analyses (%weight). This decomposed gouge material has been used for experiments on partially decomposed dolomite gouge.

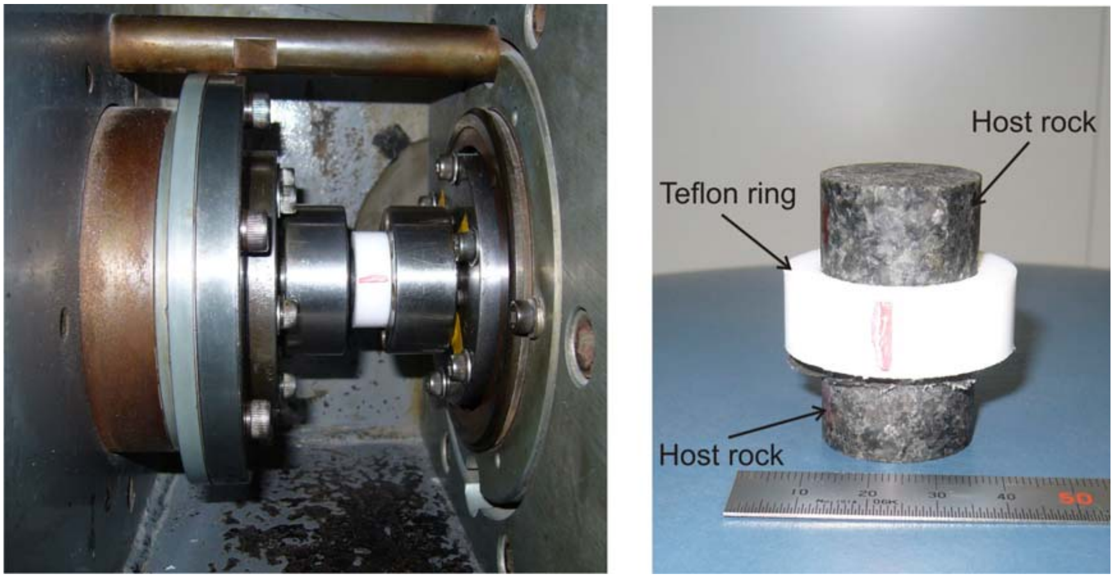

Supplementary Figure DR2: Sample assembly and experimental determination of slip rate and slip for cylindrical samples. We performed 34 experiments at room temperature and humidity conditions with a high velocity rotary shear friction apparatus (see left panel, Hirose & Shimamoto, *J. Geophys. Res.* **110**, doi:10.1029/2004JB003207, 2005). Experiments were performed on fine-grained (<100 μm), sharp-edged, gouges of (1) pure dolomite $MgCa(CO_3)_2$ (dry and saturated with 0.4ml of distilled water), (2) partially decomposed dolomite made of Mg-rich calcite $(Ca_xMg_{1-x})CO_3$ and periclase (MgO) and 3) totally decomposed dolomite made of lime (CaO) and periclase (MgO) (Supplementary Fig. 1). A synthetic fault zone was made by sandwiching an approximately 1 mm thick gouge layer between two cylindrical (25 mm in diameter) gabbro host rocks. The specimen assemblage was confined with a Teflon ring to limit gouge loss during the experiments (right panel, see Mizoguchi, et al., G*eophys. Res. Lett.* **34,** doi:10.1029/2006GL027931, 2007).

Given the cylindrical shape of the sandwiching host rocks, the determination of slip rate *V* in the gouge is problematic, since *V* increases with sample radius *r* ($V = \omega r$; ω is the rotary speed). During the experiments, the revolution rate of the motor *R* and the torque *T* are measured. It follows that the slip rate for the gouge is obtained in terms of "equivalent slip rate" V_e (see for details Shimamoto and Tsutsumi, S*truct. Geol.* **39**, 65-78, 1994; Hirose & Shimamoto, *J. Geophys. Res.* **110**, doi:10.1029/2004JB003207, 2005) by

$$V_e = \frac{4\pi Rr}{3} \qquad \text{Eq. 1.}$$

We refer the equivalent slip rate simply as slip rate *V* in the paper and, as a consequence, the slip *d* is

$$d = V_e \, t \qquad \text{Eq. 2.}$$

where *t* is the time.

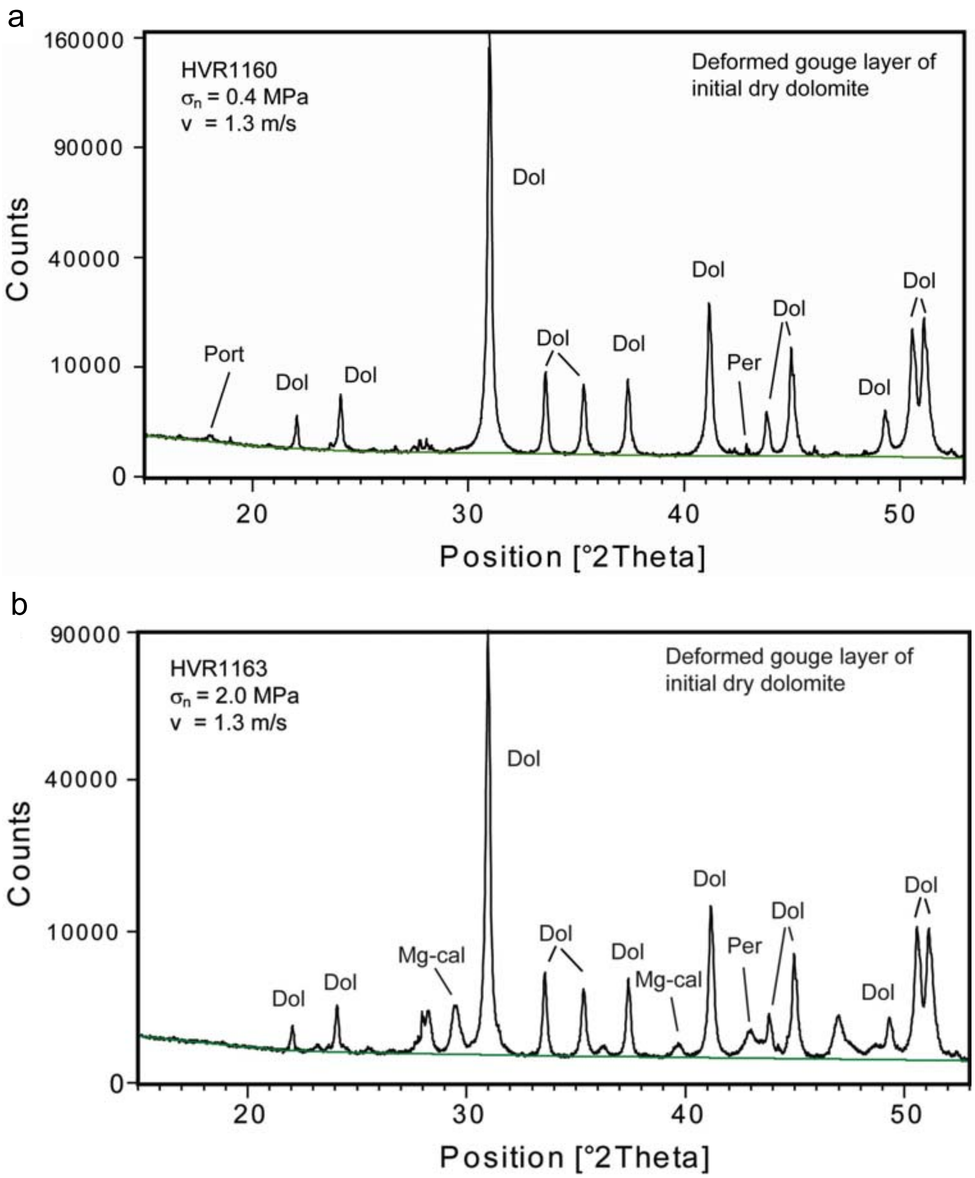

Supplementary Figure DR3: Composition of deformed gouge material. a-b. Semi-quantitative X RPD pattern (15 hours scan) carried out on the entire thickness of the deformed gouge layer report the presence of: (**a**) almost pure dolomite with traces of portlandite and periclase; (**b**) small amounts (few %) of Mg-rich calcite and periclase (i.e., the thermal decomposition products of dolomite at *T* of about 550°C). However, the amount of decomposed products is likely to be higher within and adjacent to the slip zone where most of the decomposed dolomite products are localized as shown by microstructural analyses (see Fig. 2 in the main text). The presence of minor Fluorite (CaF_2) was also detected at 2θ of about 28º.

Supplementary Table DR1 – Summary of mechanical data from all experiments performed on dry and saturated dolomite gouge, partially and totally decomposed dolomite gouge.

Sample	Lithology (gouge)	Slip rate (m/s)	d_{Tot} (m)	σ_n (MPa)	σ_{np} (MPa)	$\sigma_{n\,ss}$ (MPa)	τ_p (MPa)	$\tau_{p\,cor}$ (MPa)	$\tau_{ss\,1}$ (MPa)	$\tau_{ss\,2}$ (MPa)	τ_{mean} (MPa)	μ_p	$\mu_{p\,cor}$	μ_{ss}	D_w (m)	W_b (MJ/m^2)	T_{Dw} Av (°C)	T_{Dw} Max (°C)
Dol1176	Dolomite	0	0	1.2	-	-	-	-	-	-	-	-	-	-	-	-	-	-
Dol1166	Dolomite	0.009	0.16	1.23	1.27	1.24	0.85	-	-	1.12	0.98	0.67	-	0.90	0.067	-	24	25
Dol1169	Dolomite	0.09	4.615	1.19	1.33	1.18	1.34	-	-	0.94	1.02	1.01	-	0.80	1.08	-	78	91
Dol1168	Dolomite	0.69	19.79	1.22	1.39	1.20	1.3	-	-	0.49	0.69	0.94	-	0.40	5.41	1.10	268	324
Dol1160	Dolomite	1.3	60.91	0.43	0.6	0.41	0.62	0.59	-	0.11	0.22	1.03	0.98	0.28	30.02	3.13	275	332
Dol1161	Dolomite	1.3	41.58	0.82	0.92	0.82	0.94	0.91	-	0.20	0.31	1.02	0.98	0.24	10.65	1.86	234	283
Dol1156	Dolomite	1.3	38.25	0.81	0.86	0.80	0.76	0.73	-	0.12	0.28	0.88	0.84	0.14	24.51	4.01	314	380
Dol1158	Dolomite	1.3	33.57	1.21	1.28	1.21	1.11	1.08	0.27	0.33	0.52	0.87	0.84	0.27	5.15	1.25	270	326
Dol1157	Dolomite	1.3	40.59	1.22	1.34	1.21	1.27	1.24	0.22	0.38	0.58	0.95	0.92	0.31	6.88	2.39	342	415
Dol1159	Dolomite	1.3	18.76	1.65	1.75	1.65	1.49	1.46	0.31	0.42	0.67	0.85	0.83	0.25	4.41	1.06	318	385
Dol1167	Dolomite	1.3	36.31	1.62	1.71	1.63	1.43	1.4	0.22	0.36	0.70	0.84	0.81	0.22	4.79	1.54	345	418
Dol1165	Dolomite	1.3	46.4	1.63	1.72	1.63	1.73	1.7	-	0.28	0.66	1.01	0.98	0.17	6.58	2.4	379	460
Dol1164	Dolomite	1.3	33.81	2.03	2.11	2.08	1.84	1.81	0.21	0.45	0.81	0.87	0.86	0.22	3.05	1.3	320	387
Dol1163	Dolomite	1.3	32.72	2.07	2.17	2.07	2.19	2.16	0.24	0.36	0.85	1.01	0.99	0.17	5.62	2.63	447	543
DolSat1177	Dol. saturated	0	0	1.2	-	-	-	-	-	-	-	-	-	-	-	-	-	-
DolSat1173	Dol. saturated	1.3	43.2	0.85	0.95	0.78	1.03	0.46	0.18	-	0.39	1.08	0.48	0.23	3.44	0.69	173	208
DolSat1170	Dol. saturated	1.3	45.67	1.24	1.4	1.22	1.35	0.78	0.29	-	0.55	0.96	0.56	0.24	4.4	1.1	264	319
DolSat1171	Dol. saturated	1.3	42.11	1.64	1.8	1.67	1.46	0.89	0.32	-	0.63	0.81	0.50	0.19	3.62	1.07	274	331
DolPdc1396	Dol par dec.	0	0	1.2	-	-	-	-	-	-	-	-	-	-	-	-	-	-
DolPdc1392	Dol par dec.	1.3	26.91	1.21	1.3	1.23	1.29	1.05	-	0.33	0.59	0.99	0.81	0.27	5.05	1.25	301	364
DolPdc1393	Dol par dec.	1.3	33.92	1.22	1.26	1.23	1.14	0.9	-	0.3	0.51	0.90	0.71	0.24	7.59	1.56	318	385
DolPdc1390	Dol par dec.	1.3	29.32	1.61	1.68	1.61	1.46	1.22	0.3	0.46	0.73	0.87	0.73	0.29	5.85	2.41	394	478
DolPdc1391	Dol par dec.	1.3	27.62	2.01	2.06	2.00	1.81	1.57	0.32	0.57	0.90	0.88	0.76	0.28	3.29	1.82	366	444

Supplementary Table DR1 – Summary of mechanical data from all experiments performed on dry and saturated dolomite gouge, partially and totally decomposed dolomite gouge.

Sample	Lithology (gouge)	Slip rate (m/s)	d_{Tot} (m)	σ_n (MPa)	σ_{np} (MPa)	$\sigma_{n\,ss}$ (MPa)	τ_p (MPa)	$\tau_{p\,cor}$ (MPa)	$\tau_{ss\,1}$ (MPa)	$\tau_{ss\,2}$ (MPa)	τ_{mean} (MPa)	μ_p	$\mu_{p\,cor}$	μ_{ss}	D_w (m)	W_b (MJ/m^2)	T_{Dw} Av (°C)	T_{Dw} Max (°C)
DolTdc1192	Dol Tot dec.	1.3	22.00	1.22	1.29	1.22	0.98	-	-	0.27	-	0.76	-	0.22	9.42	4.52		
DolTdc1197	Dol Tot dec.	1.3	45.8	1.25	1.36	1.26	1.09	-	-	0.17	-	0.80	-	0.13	14.99	3.11		
DolTdc1193	Dol Tot dec.	1.3	30.56	1.62	1.69	1.64	1.27	-	-	0.54	-	0.75	-	0.33	7.04	0.92		
DolTdc1196	Dol Tot dec.	1.3	11.2	1.64	1.72	1.63	1.23	-	-	0.43	-	0.72	-	0.26	10.25	1.84		
DolTdc1194	Dol Tot dec.	1.3	46.3	2.06	2.1	2.07	1.2	-	-	0.21	-	0.57	-	0.10	14.5	4.68		
DolTdc1195	Dol Tot dec.	1.3	30.6	2.05	2.11	2.07	1.34	-	-	0.21	-	0.64	-	0.10	12.01	2.72		
Dol disp1350	Dolomite	1.3	1.58	1.18	1.24	1.18	1.25	-	-	0.72	0.80	1.01	-	0.61	-	0.22	233	281
Dol disp1351	Dolomite	1.3	2.7	1.24	1.31	1.24	1.31	-	-	0.42	0.60	1.00	-	0.34	-	0.65	237	285
Dol disp1352	Dol displ.	1.3	5.3	1.22	1.28	1.23	1.29	-	-	0.33	0.61	1.01	-	0.27	3.04	0.77	248	299
Dol disp1354	Dolomite	1.3	6.17	1.22	1.31	1.22	1.23	-	-	0.4	0.63	0.94	-	0.33	3.83	0.95	281	340
Dol disp1353	Dolomite	1.3	10.5	1.22	1.28	1.21	1.15	-	-	0.34	0.56	0.90	-	0.28	3.44	0.71	239	288

Legend: d_{Tot} = total displacement; σ_n = Normal stress; σ_{np} = Peak normal stress; σ_{ss} = Peak steady state stress τ_p = Peak shear stress; $\tau_{p\,corr}$ = Corrected peak shear stress; $\tau_{ss\,1}$ = Steady state 1 shear stress (overpressure); $\tau_{ss\,2}$ = Steady state 2 shear stress (no overpressure); τ_{mean} = Mean shear stress; μ_p = Peak friction coefficient; $\mu_{p\,corr}$ = Corrected peak friction coefficient; μ_{ss} = Steady state friction coefficient; D_w = Slip weakening distance; W_b = Breakdown work; $T_{Dw\,av}$ = Calculated average temperature for d = D_w; $T_{Dw\,Max}$ = Calculated maximum temperature for d = D_w.